

Author Manuscript

Title: Selective Hydrogen Generation from Formic Acid with well-defined PN3-Ru Complexes

Authors: Kuo-Wei Huang, Ph.D.; Yupeng Pan; Chengling Pan; Huaifeng Li; Yufan Zhang; Shixiong Min; Xunmun Guo; Bin Zheng; Hailong Chen; Addison Anders; Zhiping Lai; Junrong Zheng

This is the author manuscript accepted for publication and has undergone full peer review but has not been through the copyediting, typesetting, pagination and proofreading process, which may lead to differences between this version and the Version of Record.

To be cited as: Chem. Asian J. 10.1002/asia.201600169

Link to VoR: <http://dx.doi.org/10.1002/asia.201600169>

Selective Hydrogen Generation from Formic Acid with well-defined PN³-Ru Complexes

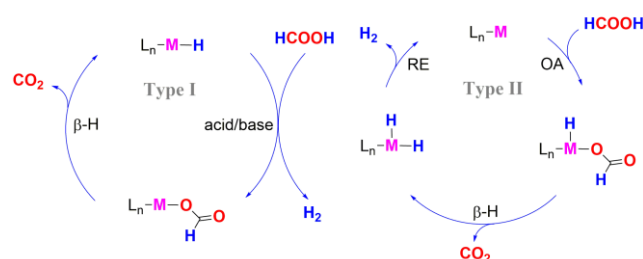
Yupeng Pan,^a Cheng-Ling Pan,^a Yufan Zhang,^b Huaifeng Li,^a Shixiong Min,^a Xunmun Guo,^b Bin Zheng,^a Hailong Chen,^b Addison Anders,^b Zhiping Lai,^a Junrong Zheng^{b,*} and Kuo-Wei Huang^{a,*}

Abstract: PN³-Pincer complexes were employed for the selective hydrogen generation from formic acid. Mechanistic studies suggest the imine arm participates in the formic acid activation/deprotonation step. A long life time of 150 hours with a turnover number over 1 million was achieved.

Hydrogen is a clean energy carrier with water as the only exhaust when combusted in engines or fuel cells. It is considered to play a critical role in the future renewable energy technologies.¹ Formic acid (FA), an adduct of CO₂ and hydrogen and a major product of biomass, has been considered as a potential liquid source and storage material for hydrogen. In particular, its volumetric hydrogen capacity reaches 53 g H₂/L, equivalent to an energy density of 1.77 kW·h/L, making it attractive for automotive and mobile applications.² A sustainable and reversible energy storage and utilization cycle can be envisioned by combining CO₂ and H₂ into formic acid to store hydrogen and remove CO₂, and decomposing formic acid to release hydrogen.³

To release hydrogen under mild conditions, homogeneous or heterogeneous catalysts are used to decompose formic acid. Towards the goal of industrially viable applications, this approach faces a couple of challenges. In many catalytic systems, trace amount of CO, which can poison the catalyst of hydrogen fuel cells, is generated as a by-product. The lifetimes (turnover number (TON)) of the catalysts are in general not sufficiently long, because of various reasons, e.g. instability to moisture, air or acid or other trace amount of impurities which exists in most formic acid supplies.

The decomposition of FA to H₂ and CO₂ is thermodynamically favored, but the energy barrier is high and the selectivity is poor due to the formation of H₂O and CO in the absence of a suitable catalyst. H₂ and CO₂ generation from FA has been studied several decades ago,⁴ but the potential of utilizing CO₂ as a H₂ storage material was not fully recognized until recently.⁵ A number of homogeneous and heterogeneous



Scheme 1. General strategies for selective hydrogen generation from formic acid.

catalyst systems have been developed for the generation of H₂ from FA.⁶ Reactions that give significantly enhanced turnover frequencies (TOFs) and turnover numbers (TONs) were achieved by using the FA/NEt₃ azeotrope or FA/formate mixtures. A few molecular catalysts also show good activities in the absence of base additives.^{6f, 6m, 6x, 6z, 6ab, 6ac} Examples of very high TONs were reported recently by the groups of Beller (TON > 1,000,000)^{6y} and Li (TON of 2,400,000),^{6ac} although the detailed mechanisms for the high activity and selectivity are not clear. It has been suggested that metal hydride groups can serve as a base in some of these external base-free systems, while in other cases cooperative ligands play the role as a base.

Two general strategies can be considered for selective hydrogen generation from formic acid (**Scheme 1**). One starts with a metal hydride species which can react with the proton of a formic acid molecule to produce H₂ and a metal formate intermediate, a typical acid and base reaction between metal hydrides and a proton source. The catalytic cycle can be completed with the β -hydride elimination (β -H) of the formate ligand to regenerate the metal hydride species. One potential risk of this model is the sensitivity of the catalyst toward water. The other type starts with the oxidative addition (OA) of formic acid to a reduced metal complex to form a hydridometal formate complex which can then undergo the β -hydride elimination to give a dihydride intermediate. It can be followed by the reductive elimination (RE) of the two hydride ligands to give hydrogen and regenerate the reduced metal complex. This type of compounds may be reactive toward oxygen and the reduced metal center may facilitate the oxidation addition of formyl C-H bond of formic acid to the metal leading to a decarbonylation reaction. Thus, to achieve a high TON in a practical fashion, the stability toward water is essential as common formic acid typically contains certain amounts of water; and in order to avoid the undesired CO formation, reduced metal species is better excluded from the catalytic cycle.

[a] King Abdullah University of Science and Technology (KAUST), Division of Physical Sciences and Engineering, Thuwal 23955-6900, Saudi Arabia. Email: hkw@kaust.edu.sa (K.-W.H.)

[b] Department of Chemistry, Rice University, Houston, TX 77005, USA. Email: junrong@rice.edu (J.Z.)

Supporting information for this article is given via a link at the end of the document.

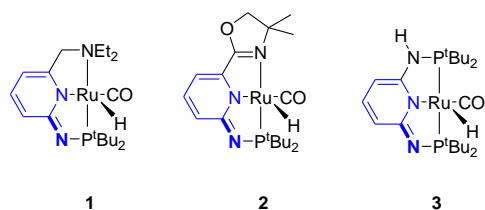


Figure 1. A new class of PN³-Ru complexes.

These previous encouraging observations and the mechanistic consideration for a highly selective and active catalyst toward hydrogenation generation from FA prompted us to evaluate the catalytic activity of Ru complexes bearing a dearomatized pyridine moiety and an imine arm. Herein, we report a rationally designed catalyst with high activity and selectivity for hydrogen generation from FA under mild conditions (**Fig. 1**). These catalysts are not air or water sensitive and no detectible CO is generated from the hydrogen generation reaction. The best catalyst is active (turnover frequency (TOF) > 7,000 hr⁻¹) over a very long lifetime of 9,000 minutes with a turnover number more than 1 million at 90 °C. The reaction setup is simple and no sophisticated devices are required. These are favored properties for various applications. Mechanistic insights from NMR studies are also presented.

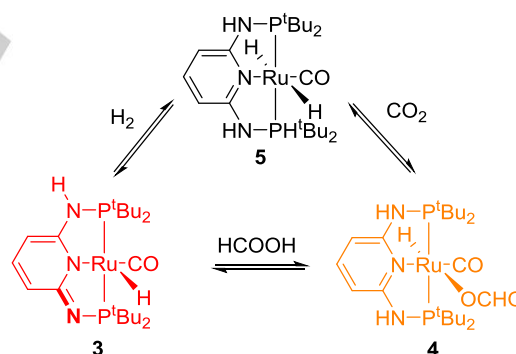
We have recently developed a new class of dearomatized pyridine-based pincer complexes through the deprotonation of one NH-P^tBu₂ arm (**Fig. 1**). This change has resulted in a huge impact on the catalytic functions and stability of the complexes compared to their methylene counterpart developed by Milstein.⁷ It was found that these new complexes are air- and moisture-stable, and they catalyze reactions where the analogs with a CH₂ spacer show limited activities. For examples, the Milstein's catalyst catalyzes the dehydrogenative acylation of amines, but our catalysts catalyze the selective dehydrogenation (oxidation) of benzylamines into imines.⁸ Our catalysts efficiently catalyze the hydrogenation of esters under mild conditions even in the presence of water.⁹ These surprising discoveries strongly suggest that the N-H arm change not only the thermodynamic stability of these complexes toward water but also the kinetic behavior. Indeed, our recent studies indicated that our catalysts go through a different mechanism for hydrogen activation where two water molecules (or protic molecules) are needed as the proton shuttle(s).⁹⁻¹⁰ These exciting and unexpected results of the catalysts based on our PN³-pincer ligands imply that they could be suitable for catalyzing the dehydrogenation reaction of FA. To our delight, promising catalytic performances were achieved under base-free conditions in DMSO for **3** among three PN³-pincer Ru complexes (**Table 1**), while none to low activities were observed in toluene, suggesting the reaction is sensitive to the selection of the solvent medium. Further solvent screening revealed that the highest activity was achieved in DMSO (Entries 5-9, **Table 1**). Complex **3** aged in air for one month showed no apparent difference in the catalytic activity (entry 10, **Table 1**). It is also very important to note that no formation of CO was detected, indicating that the purity of the regenerated gas is suitable for the use in hydrogen fuel cells (see SI)

To gain insight into the high reactivity and selectivity, a series of NMR studies and model reactions were conducted. The ¹H NMR spectrum of **3** in DMSO-*d*₆ shows three sets of sp² C-H signals at δ 5.57 (d), 5.94 (d) and 6.85 (t) ppm, indicative of

Table 1. Ru(II)-catalyzed hydrogen production from formic acid.^[a]

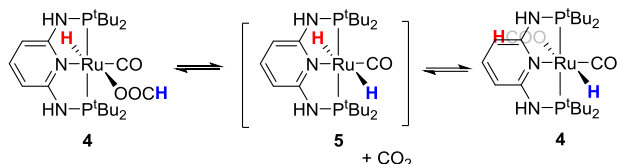
		HCOOH $\xrightarrow{\text{Cat.}}$ H ₂ + CO ₂		
Entry	Solvent	Cat.	T (°C)	TON
1	DMSO	1	50	9800
2	Toluene	1	50	-
3	DMSO	2	50	2400
4	Toluene	2	50	-
5	DMSO	3	50	95000
6	Toluene	3	50	2000
7	MeCN	3	50	4800
8	DMF	3	50	3500
9	THF	3	50	3600
10 ^[b]	DMSO	3	50	95000

[a] Reaction conditions: Ru complex (1.0 μmol in 5.0 mL of respective solvent), 95% commercial formic acid was injected by the microinjector (see supporting information). TON was estimated based on the H₂ collected by water displacement, with the solvent and water vapors neglected. Carbon dioxide was absorbed by a saturated solution of potassium hydroxide. [b] Catalyst **3** was exposed to the air for one month.



Scheme 2. Plausible mechanism for the hydrogenation of CO₂ and production of H₂ from formic acid catalyzed by complex **3**.

the dearomatization of the central pyridine ring. These results are consistent with two phosphorus signals observed in the ³¹P NMR with an apparent triplet for a hydride at δ = -26.43 ppm in ¹H NMR. The presence of water as indicated by a peak at δ = 3.33 ppm in the ¹H NMR showed that this dearomatized Ru(II) complex did not react with H₂O in DMSO even when heating in an oil bath at 100 °C for 12 hours! This observation supports **3**'s stability towards water. Upon treatment with 1.5 equivalents of FA, the sp² C-H signals were shifted to downfield at δ 6.33 and 7.27 ppm, indicating that the imine arm was re-protonated leading to the rearomatization of the pyridine ring. A new and more downfield hydride signal was formed at δ -16.94 ppm in ¹H NMR, consistent with the presence of a ligand trans to H.



Scheme 3. Proposed mechanism for the exchange of Ru-H and Ru-OOCH signals.

This ligand was confirmed to be a formate group owing to the observation of a formate signal at δ 165.8 ppm in ^{13}C NMR and a formyl hydrogen at δ 8.39 ppm in ^1H NMR. The formation of hydridoruthenium formate **4** was thus assigned accordingly (**Scheme 2**). The formation of **4** was also accompanied by the disappearance of **3**'s reddish orange color in the solution (**SFigure 1**). It was noted that intermediate **4** slowly decomposed with production of H_2 and CO_2 and the color of the solution changed from very pale yellow back to reddish orange, indicating the regeneration on **3**, which was also confirmed by NMR.

The plausible mechanism for the catalytic transformation includes three steps: the protonation of the imine arm of the dearomatized pincer complex (**3**) to intermediate **4**, the decomposition of formate **4** with liberation of CO_2 , and the elimination of hydrogen to regenerate the catalyst. During the whole process, the oxidation state of Ru remains II. While the proposed dihydride species (**5**) was not seen during the formic acid dehydrogenation reaction monitored by ^1H NMR, complex **5** can be formed *in situ* when hydrogen was introduced to the DMSO solution of **3**. It is also very important to note that, in dry C_6D_6 solution, no reaction between complex **3** and H_2 was observed. However, when wet C_6D_6 was used, instant conversion of **3** and H_2 into dihydride **5** was achieved. These results are consistent with our earlier studies which suggest water (protic) molecules are needed for hydrogenation of the dearomatized $\text{PN}^3\text{-Ru}$ complexes.^{7a} Upon treatment of CO_2 , **5** was converted to formate **4**. Moreover, exchange signals between the Ru-H and Ru-OOCH was observed under 2D NOESY experiments (See SI), suggesting the possible equilibrium between intermediate **4** and dihydride **5** and CO_2 (Scheme 3), strongly supporting the role of **5** in the proposed catalytic process and implying that the hydrogen elimination is unlikely the rate determining step. When DCOOH was used, not only the initial rate decreased by about 5 times, formation of H_2 and HD were also observed in the ^1H NMR, indicating that the β -hydride elimination of the formate group may be rate-determining and the deuterium scrambling is likely a result of fast equilibrium between species **3-5**, H_2 (HD and D_2), CO_2 , and HCOOH (DCOOH and DCOOD).

Table 2. Effect of base on the efficiency of formic acid dehydrogenation.^[a]

Entry	Solvent	Additive	T (°C)	TOF (h ⁻¹)	TON
1	DMSO	Et_3N	90	7333	1,100,000
2	DMSO	Na_2CO_3	90	13123	350,000
3	DMF	Et_3N	90	31000	93,000

[a] Reaction conditions: Ru complex **3** (1.0 μmol), TON was estimated based on the gas produced. Base loading: NEt_3 (1.5 mL) or Na_2CO_3 (0.624 g), FA was injected at the specified rate (see supporting information).

It has been shown that the presence of a base, e.g. Na_2CO_3 and NEt_3 , could enhance the activities and life time of the catalysts for formic acid dehydrogenation (Table 2).^{5b, 6r, 6y, 11} High activities were identified with an average TOF of 7,300 h⁻¹ and a TON of 1,100,000 at 90 °C. Interestingly, in the presence of a more general base, Na_2CO_3 , the performance of the catalyst **3** showed a TOF of ~13,100 h⁻¹ and a TON of 350,000. Unfortunately, attempts in pushing the faster reaction rates, e.g. using DMF as the solvent in the presence of NEt_3 with an increased FA injection rate, only resulted in a slightly enhanced TOF of 31,000h⁻¹ with a significantly shorter life time. These results suggest that the stability of the catalyst greatly depends on the balance between the base and acid. It was found that catalyst **3** indeed decomposed in high concentration of formic acid to release free phosphines evidenced in the ^{31}P NMR (δ = 56.9 ppm), presumably due to the over protonation of the amine arm which led to hydrolysis of the N-P bonds.¹² The N-H arms may play a potential role to modulate the acidity of the reaction environment.

In conclusion, we have developed an active and selective catalyst for hydrogen production from FA. The reaction starts with the protonation of the dearomatized ligand and during the process the oxidation state of the Ru center does not change. This avoids the decarbonylation process and thus makes the reaction perfectly selective without the formation of CO. The enhanced water and air stabilities are likely realized by the tridentate binding of the ligand, the +2 oxidation state of Ru(II), and the bulky steric effect of the t-butyl groups. The ability of tuning the local environment by the two N-H arms may also contribute to the long lifetime of the catalyst. This mechanism significantly reduces the chance for protons to attack the coordination atoms and the metal center under well-controlled FA injection rate, and therefore diminishes the decomposition of the catalyst induced by the attack of protons. The tolerance to water of **3** may enable the use of practically feasible hydrogen generation from FA.

K.-W.H. acknowledges the financial support from KAUST and a SABIC Chair Professorship. J.Z. thanks the supports from NSF (CHE-1503865), the Welch foundation under Award No. C-1752, Packard fellowship, and Sloan fellowship. Y.Z. thanks a Schlumberger future faculty award.

1. a) Lewis, N. S.; Nocera, D. G., *PNAS* **2006**, *103*, 15729-15735; b) Whitesides, G. M.; Crabtree, G. W., *Science* **2007**, *315*, 796-798; c) Moriarty, P.; Honnery, D., *Int. J. Hydrogen Energy* **2009**, *34*, 31-39; d) Moriarty, P.; Honnery, D., *Int. J. Hydrogen Energy* **2010**, *35*, 12374-12380; e) Turner, J. A., *Science* **2004**, *305*, 972-974; f) Armaroli, N.; Balzani, V., *ChemSusChem* **2011**, *4*, 21-36.
2. a) Felderhoff, M.; Weidenthaler, C.; von Helmolt, R.; Eberle, U., *Phys. Chem. Chem. Phys.* **2007**, *9*, 2643-2653; b) Sakintuna, B.; Lamari-Darkrim, F.; Hirscher, M., *Int. J. Hydrogen Energy* **2007**, *32*, 1121-1140; c) Yueruem, Y.; Taralp, A.; Veziroglu, T. N., *Int. J. Hydrogen Energy* **2009**, *34*, 3784-3798; d) Suh, M. P.; Park, H. J.; Prasad, T. K.; Lim, D.-W., *Chem. Rev.* **2012**, *112*, 782-835.
3. a) Enthaler, S., *ChemSusChem* **2008**, *1*, 801-804; b) Joo, F., *ChemSusChem* **2008**, *1*, 805-808; c) Grasemann, M.; Laurenczy, G., *Energy Environ. Sci.* **2012**, *5*, 8171-8181; d) Mura, M. G.; De Luca, L.; Giacomelli, G.; Porcheddu, A., *Adv. Synth. Catal.* **2012**, *354*, 3180-3186.
4. a) Strauss, S. H.; Whitmire, K. H.; Shriver, D. F., *J. Organomet. Chem.* **1979**, *174*, C59-C62; b) Paonessa, R. S.; Troglor, W. C., *J. Am. Chem. Soc.* **1982**, *104*, 3529-3530; c) Wiener, H.; Sasson, Y.; Blum, J., *J. Mol. Catal.* **1986**, *35*, 277-284; d) Gao, Y.; Kuncheria, J. K.; Jenkins, H. A.; Puddephatt, R. J.; Yap, G. P. A., *J. Chem. Soc., Dalton Trans.* **2000**, 3212-3217; e) Ogo, S.; Nishida, H.; Hayashi, H.; Murata, Y.; Fukuzumi, S., *Organometallics* **2005**, *24*, 4816-4823.
5. a) Fellay, C.; Dyson, P. J.; Laurenczy, G., *Angew. Chem. Int. Ed.* **2008**, *47*, 3966-3968; b) Loges, B.; Boddien, A.; Junge, H.; Beller, M., *Angew. Chem., Int. Ed.* **2008**, *47*, 3962-3965.
6. a) Fukuzumi, S.; Kobayashi, T.; Suenobu, T., *ChemSusChem* **2008**, *1*, 827-834; b) Zhou, X.; Huang, Y.; Xing, W.; Liu, C.; Liao, J.; Lu, T., *Chem. Commun.* **2008**, 3540-3542; c) Boddien, A.; Loges, B.; Junge, H.; Gaertner, F.; Noyes, J. R.; Beller, M., *Adv. Synth. Catal.* **2009**, *351*, 2517-2520; d) Ojeda, M.; Iglesia, E., *Angew. Chem. Int. Ed.* **2009**, *48*, 4800-4803; e) Ting, S.-W.; Cheng, S.; Tsang, K.-Y.; van der Laak, N.; Chan, K.-Y., *Chem. Commun.* **2009**, 7333-7335; f) Himeda, Y., *Green Chem.* **2009**, *11*, 2018-2022; g) Boddien, A.; Loges, B.; Gaertner, F.; Torborg, C.; Fumino, K.; Junge, H.; Ludwig, R.; Beller, M., *J. Am. Chem. Soc.* **2010**, *132*, 8924-8934; h) Bulushev, D. A.; Beloshapkin, S.; Ross, J. R. H., *Catal. Today* **2010**, *154*, 7-12; i) Huang, Y.; Zhou, X.; Yin, M.; Liu, C.; Xing, W., *Chem. Materials* **2010**, *22*, 5122-5128; j) Scholten, J. D.; Precht, M. H. G.; Dupont, J., *ChemCatChem* **2010**, *2*, 1265-1270; k) Majewski, A.; Morris, D. J.; Kendall, K.; Wills, M., *ChemSusChem* **2010**, *3*, 431-434; l) Zhou, X.; Huang, Y.; Liu, C.; Liao, J.; Lu, T.; Xing, W., *ChemSusChem* **2010**, *3*, 1379-1382; m) Boddien, A.; Mellmann, D.; Gaertner, F.; Jackstell, R.; Junge, H.; Dyson, P. J.; Laurenczy, G.; Ludwig, R.; Beller, M., *Science* **2011**, *333*, 1733-1736; n) Solymosi, F.; Koos, A.; Liliom, N.; Ugrai, I., *J. Catal.* **2011**, *279*, 213-219; o) Tanaka, R.; Yamashita, M.; Chung, L. W.; Morokuma, K.; Nozaki, K., *Organometallics* **2011**, *30*, 6742-6750; p) Tedsree, K.; Li, T.; Jones, S.; Chan, C. W. A.; Yu, K. M. K.; Bagot, P. A. J.; Marquis, E. A.; Smith, G. D. W.; Tsang, S. C. E., *Nature Nanotech.* **2011**, *6*, 302-307; q) Luo, Q.; Feng, G.; Beller, M.; Jiao, H., *J. Phy. Chem. C* **2012**, *116*, 4149-4156; r) Hull, J. F.; Himeda, Y.; Wang, W.-H.; Hashiguchi, B.; Periana, R.; Szalda, D. J.; Muckerman, J. T.; Fujita, E., *Nat. Chem.* **2012**, *4*, 383-388; s) Mori, K.; Dojo, M.; Yamashita, H., *ACS Catal.* **2013**, *3*, 1114-1119; t) Gan, W.; Snelders, D. J. M.; Dyson, P. J.; Laurenczy, G., *ChemCatChem* **2013**, *5*, 1126-1132; u) Wang, Z.-L.; Yan, J.-M.; Ping, Y.; Wang, H.-L.; Zheng, W.-T.; Jiang, Q., *Angew. Chem. Int. Ed.* **2013**, *52*, 4406-4409; v) Wang, Z.-L.; Yan, J.-M.; Wang, H.-L.; Ping, Y.; Jiang, Q., *J. Mater. Chem. A* **2013**, *1*, 12721-12725; w) Zell, T.; Butschke, B.; Ben-David, Y.; Milstein, D., *Chem. Eur. J.* **2013**, *19*, 8068-8072; x) Oldenhof, S.; de Bruin, B.; Lutz, M.; Siegler, M. A.; Patureau, F. W.; van der Vlugt, J. I.; Reek, J. N. H., *Chem. Eur. J.* **2013**, *19*, 11507-11511; y) Sponholz, P.; Mellmann, D.; Junge, H.; Beller, M., *ChemSusChem* **2013**, *6*, 1172-1176; z) Barnard, J. H.; Wang, C.; Berry, N. G.; Xiao, J.-L., *Chem. Sci.* **2013**, *4*, 1234-1244; aa) Filonenko, G. A.; van Putten, R.; Schulp, E. N.; Hensen, E. J. M.; Pidko, E. A., *ChemCatChem* **2014**, *6*, 1526-1530; ab) Bielinski, E. A.; Lagaditis, P. O.; Zhang, Y.; Mercado, B. Q.; Würtele, C.; Bernskoetter, W. H.; Hazari, N.; Schneider, S., *J. Am. Chem. Soc.* **2014**, *136*, 10234-10237; ac) Wang, Z.; Lu, S.-M.; Li, J.-L.; Wang, J.; Li, C., *Chem. Eur. J.* **2015**, *21*, ad) Chen, H.-T.; Wang, C.; Wu, X.-F.; Jiang, X.; Catlow, C. R. A.; Xiao, J.-L., *Chem. Eur. J.* **2015**, *21*, 16564-16577.
7. a) Gunanathan, C.; Milstein, D., *Chem. Rev.* **2014**, *114*, 12024-12087; b) Li, H.; Zheng, B.; Huang, K.-W., *Coord. Chem. Rev.* **2015**, *293-294*, 116-138.
8. a) Chen, T.; He, L.-P.; Gong, D.; Yang, L.; Miao, X.; Eppinger, J.; Huang, K.-W., *Tetrahedron Lett.* **2012**, *53*, 4409-4412; b) He, L.-P.; Chen, T.; Gong, D.; Lai, Z.; Huang, K.-W., *Organometallics* **2012**, *31*, 5208-5211; c) He, L.-P.; Chen, T.; Xue, D.-X.; Eddaoudi, M.; Huang, K.-W., *J. Organomet. Chem.* **2012**, *700*, 202-206.
9. Chen, T.; Li, H.; Qu, S.; Zheng, B.; He, L.; Lai, Z.; Wang, Z.-X.; Huang, K.-W., *Organometallics* **2014**, *33*, 4152-4155.
10. Qu, S.; Dang, Y.; Song, C.; Wen, M.; Huang, K.-W.; Wang, Z.-X., *J. Am. Chem. Soc.* **2014**, *136*, 4974-4991.
11. Mellone, I.; Peruzzini, M.; Rosi, L.; Mellmann, D.; Junge, H.; Beller, M.; Gonsalvi, L., *Dalton Trans.* **2013**, *42*, 2495-2501.
12. Benito-Garagorri, D.; Mereiter, K.; Kirchner, K., *Eur. J. Inorg. Chem.* **2006**, 4374-4379.

Experimental Details

General Procedures

All operations were carried out under an atmosphere of dry argon by using Schlenk techniques or glovebox under argon. Chemicals were purchased from commercial sources and used without purification, unless otherwise noted. All the solvents used for reactions were distilled under argon after drying over an appropriate drying agent or passed through solvent purification columns. ^1H and ^{13}C NMR spectra were recorded on a Bruker 400 MHz or 600 MHz spectrometer at 400 MHz and 100 MHz or 600 MHz and 125 MHz, respectively. All chemical shifts were reported as δ in ppm with reference to the residual solvent resonance of the deuterated solvents for proton and carbon chemical shifts, and to external H_3PO_4 (85%) for phosphorus chemical shifts. Elemental analyses were carried out on a Flash 2000 elemental analyzer. The X-ray diffraction data were collected using a Bruker-AXS KAPPA-APEXII CCD diffractometer. Dearomatized ruthenium complexes **1-3** were synthesized according to the literature.^[S1] An improved procedure for compound **3** was developed.

Procedure for Catalyst and solvent testing for Decomposition of Formic Acid (Table 1 and STable 1).

Formic acid decomposition experiments were carried out in a two-necked round flask equipped with a reflux condenser and a magnetic stirrer at 50 °C. The catalyst (1.0 μmol) was dissolved in 5.0 mL of the respective solvent. Formic acid (1.20 mL) was added dropwise to the solution via a syringe pump in one hour. The generated H_2 was collected by water displacement and TON was calculated accordingly. In the case of entries 5 and 10 of Table 1, the previous portion of formic acid was fully consumed in 18 hours before the addition of a new portion of formic acid (1.20 mL).

General Procedure for Decomposition of Formic Acid.

Formic acid decomposition experiments were carried out in a two-necked round flask equipped with a reflux condenser and a magnetic stirrer at appropriate temperature. The catalyst (5.27 mg, 10 μmol) was dissolved in DMSO (or other solvent such as toluene) (10.0 mL). In a typical procedure, the solution of catalyst (1.0 mL, 1.0 μmol) was injected into a two-necked round flask and formic acid was added at a constant rate, which was determined so that the rates of consumption and addition of formic acid stayed the same; please refer to the description in Figures S17 and S18. The initial TOF was not affected by the catalyst loading of 0.5-5.0 μmol (in 1.7 mL of DMSO and 1.5 mL of NEt_3). The typical induction time was 1 min, the evolution of the generated gas was observed and could be monitored using an ADM 2000 Flowmeter simultaneously. The data was collected every 2 seconds to the computer by the ADM tracer. The ratio of H_2 and CO_2 was 1:1, which was confirmed by GC analysis. The amount of H_2 was confirmed via the water displacement method. To quantify the gas products for the formic acid

decomposition experiments, an on-line pre-calibrated gas chromatograph (Agilent 7890B) (H_2 , CO , CH_4 , CO_2) were employed, which was equipped with the following two channels: 1) two HayeSep Q columns and a 13x molecular sieves with a thermal conductivity detector using He as a carrier gas for CO_2 and CO analysis, and 2) a HayeSep Q and a 13x molecular sieves with a thermal conductivity detector using Ar as a carrier gas for H_2 analysis. The minimum detection limit for the gas products was 10 ppm. After an initial reaction time of 1 min, the gas produced was analyzed by purging the produced gas directly to the on-line GC and the analysis starts every 15 min.

Improved procedure for the Synthesis of Complex 3.

The THF solution of **PN³P-Ru** (281.6 mg, 0.5 mmol) was added dropwise to the THF solution of one equivalents KO^tBu (56.0 mg, 0.5 mmol), and the reaction mixture was stirred at room temperature for 2h. After filtered, the volatiles were removed under vacuum, and the residue was washed with 3×3 mL of pentane. Evaporation of the red residue under vacuum gave compound **3** as a red solid (240.6 mg, 92% yield).^[S1] Its ^1H NMR and ^{31}P NMR in wet $\text{DMSO-}d_6$ indicated its stability in the presence of water (Fig. S3 and S4).

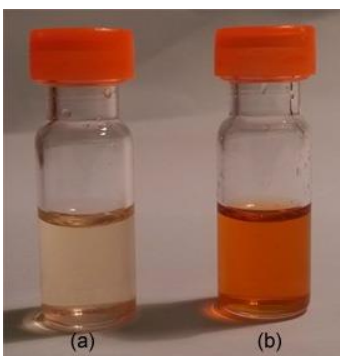


Figure S1. (a) 3 hours after the addition of FA into the DMSO solution of **3** in a closed system (b) 3 hours after the addition of FA into the DMSO solution of **3** in an open system.

Treatment of **3** with H_2 .

To a J-Young NMR tube was added ruthenium **3** (5.3 mg, 0.01mmol) and $\text{DMSO-}d_6$ (0.5 mL) under an argon atmosphere; the tube was then evacuated and refilled with H_2 in 3 freeze-pump-thaw cycles. The mixture was placed at 20°C and monitored via ^1H and ^{31}P NMR spectroscopy (Fig. S5 and S6). ^1H NMR ($\text{DMSO-}d_6$, 400 MHz) δ 6.96 (t, $J = 8.0$ Hz, 1H, -Py), 6.01(d, $J = 8.0$ Hz, 2H, -Py), 1.35-1.38(m, 36H, - ^tBu), -6.15 (dd, $J = 20.0$ Hz, 2H, -RuH). ^{31}P NMR ($\text{DMSO-}d_6$,

162.5 MHz) 154.30. Excess free H₂ was present as a singlet at 4.60 ppm. This reaction was not observed in the dry C₆D₆ (Fig. S7 and S8).

Treatment of **5** with ¹³CO₂.

To a DMSO-*d*₆ (0.5 mL) solution of *trans*-Ru(H)₂ **5** made *in situ* in a J-Young NMR tube was filled with 1 atom of ¹³CO₂ in 2 freeze-pump-thaw cycles. The reaction was then monitored via ¹³C, ¹H and ³¹P NMR spectroscopy. The hydride were observed at δ -16.86 ppm compared with the previous δ -6.15 ppm from **5** in ¹H NMR spectrum. Intermediate **4** exhibited a resonance at δ 8.34 ppm (*J*_{C-H} = 176 Hz) for the Ru-O¹³CHO in the ¹H NMR spectrum. The resonance at δ 166.4 ppm was confirmed for the formate group in the ¹³C NMR analysis (ns = 512). ¹H NMR (DMSO-*d*₆, 400 MHz) δ 8.34(*J*_{C-H} = 176 Hz, 1H, -CHO), 8.07(s, 2H, -NH), 7.28(t, *J* = 8 Hz, 1H, -Py), 6.30(d, *J* = 8.0 Hz, 2H, -Py), 1.22-1.37(m, 36H, -^tBu), -16.86 (br, 1H, -RuH). ³¹P NMR (DMSO-*d*₆, 162.5 MHz) 133.5. ¹³C NMR (DMSO-*d*₆, 100 MHz, ns=512) 124.2(free CO₂), 166.4 (-CHO) (Fig. S9-11).

Treatment of **3** with HCOOH.

To a DMSO-*d*₆ (0.5 mL) solution of **3** (20.2 mg) in a J-Young NMR tube, 1.5 equivalents of formic acid (2.15 μL) was added under air. The reaction was monitored by NMR analysis, indicating the formation of intermediate **4** (but no ¹³C labelling, Fig. S12). The 2D NOESY suggested the proton exchange between the H₂O and the -NH functioned groups and the Ru-H with the -OCHO group (Fig. S13).

Treatment of **3** with excess HCOOD.

To a C₆D₆ (0.5 mL) solution of **3** (20.2 mg) in a J-Young NMR tube, 6.0 equivalents of HCOOD (8.80 μL) was added at room temperature. Reaction was monitored by NMR analysis, showing H-D scrambling ((Fig. S14).

Reference

S1. He, L.; Chen, T.; Gong, D.; Lai, Z.; Huang, K. W. *Organometallics*, 2012, **31**, 5208-5211.

STable 1: Effect of various solvents on the efficiency of formic acid dehydrogenation.^[a]

Entry	Solvent	T (°C)	TOF (h)	TON
1 ^b	DMSO	50	2380	95000
2	CH ₃ CN	50	1100	4800
3	DMF	50	900	3500
4	Toluene	50	440	2000
5	THF	50	890	3600

^[a] Reaction conditions: Ru complex **3** (1.0 μmol, in the respective solvent). FA was injected by the microinjector. TON was estimated based on the produced H₂ by water displacement. Carbon dioxide was absorbed by a saturated solution of KOH. ^[b] **3** was exposed to the air for one month (Entry 10 n Table 1).

STable 2: Effect of lower temperatures.^[a]

Entry	Solvent	T (°C)	TON
1 ^b	DMSO	50	~250,000
2 ^b	DMSO	60	~370,000

^[a] Reaction conditions: Ru complex **3** (1.0 μmol), TON was estimated based on the gas produced. Base loading: NEt₃ (1.5 mL). FA was injected at the specified rate. ^[b] The reaction was stopped after 100 hours.

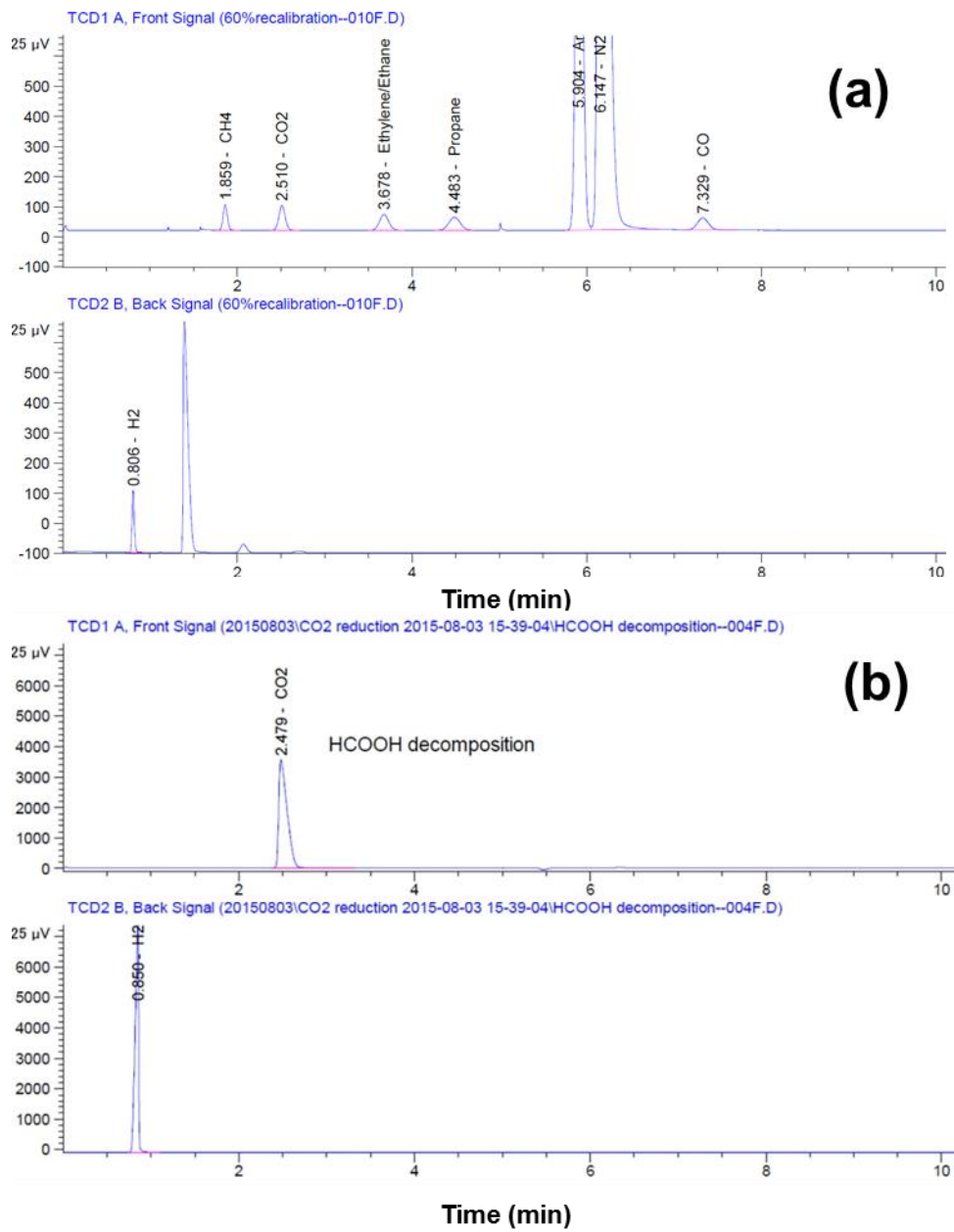
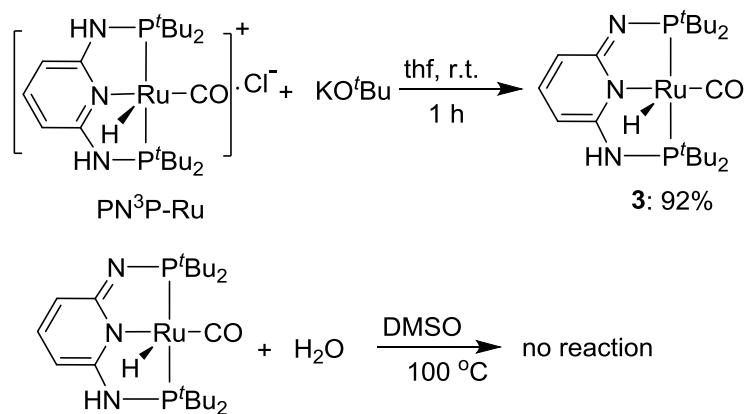
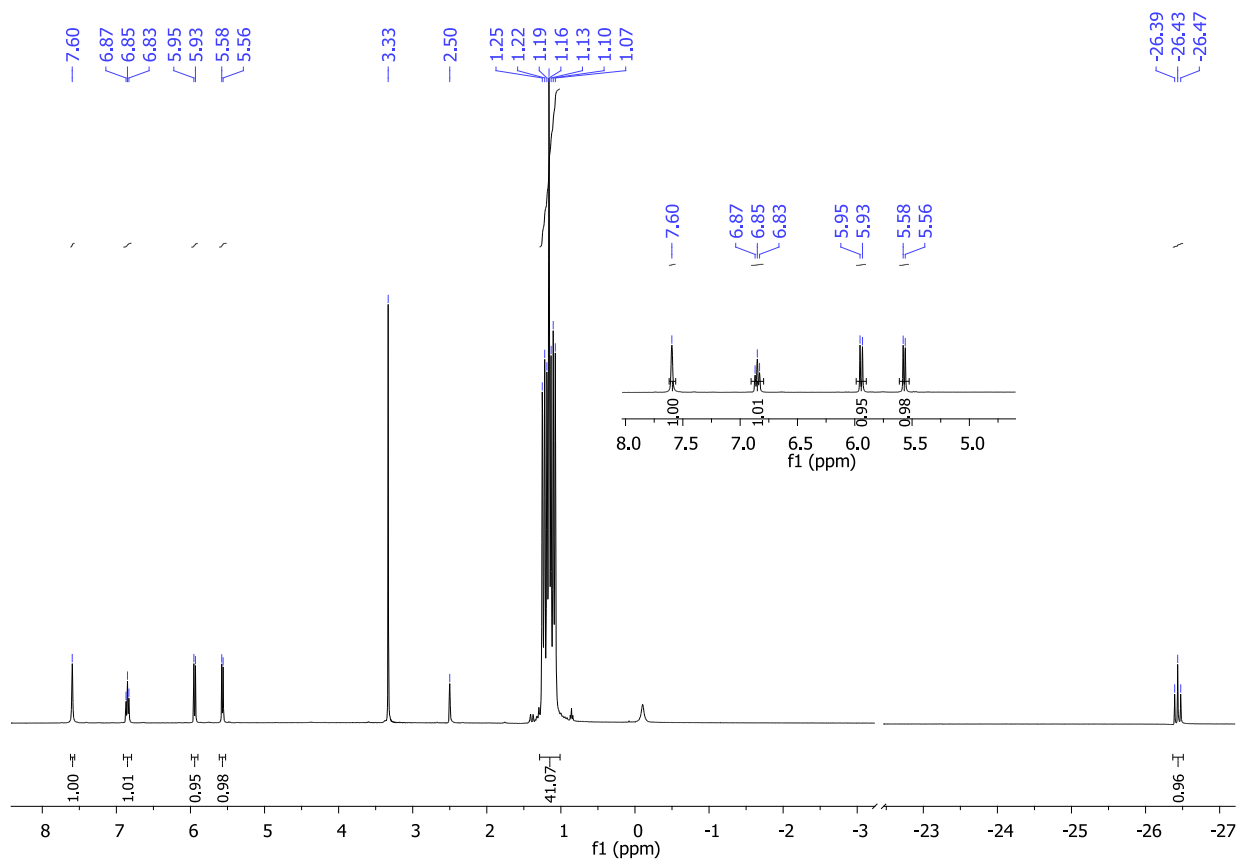


Figure S2. Composition analysis of the evolved gas mixture by GC.



Scheme S1

Figure S3. ^1H NMR spectrum of **3** in $\text{DMSO}-d_6$ (400 MHz, 25 °C).

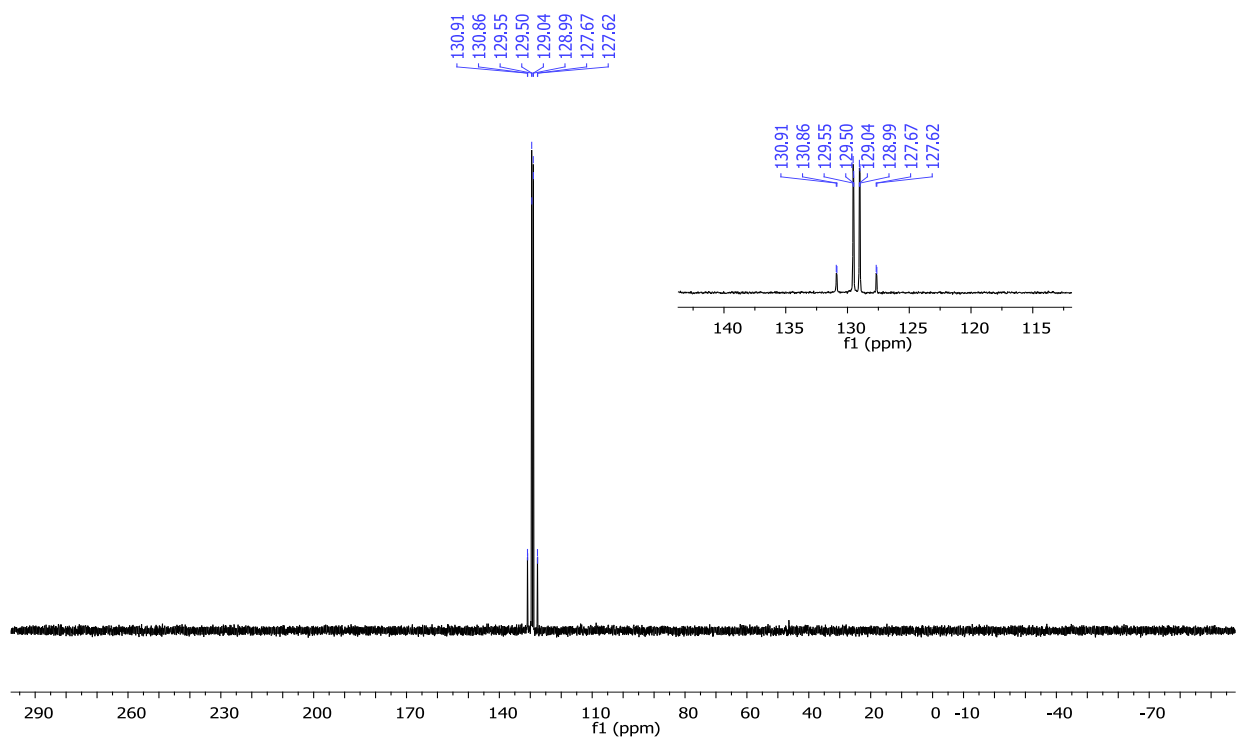
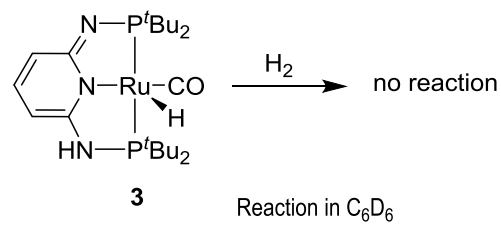
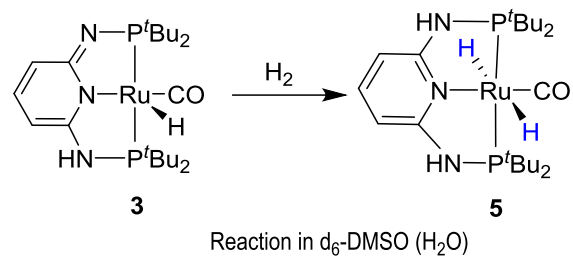
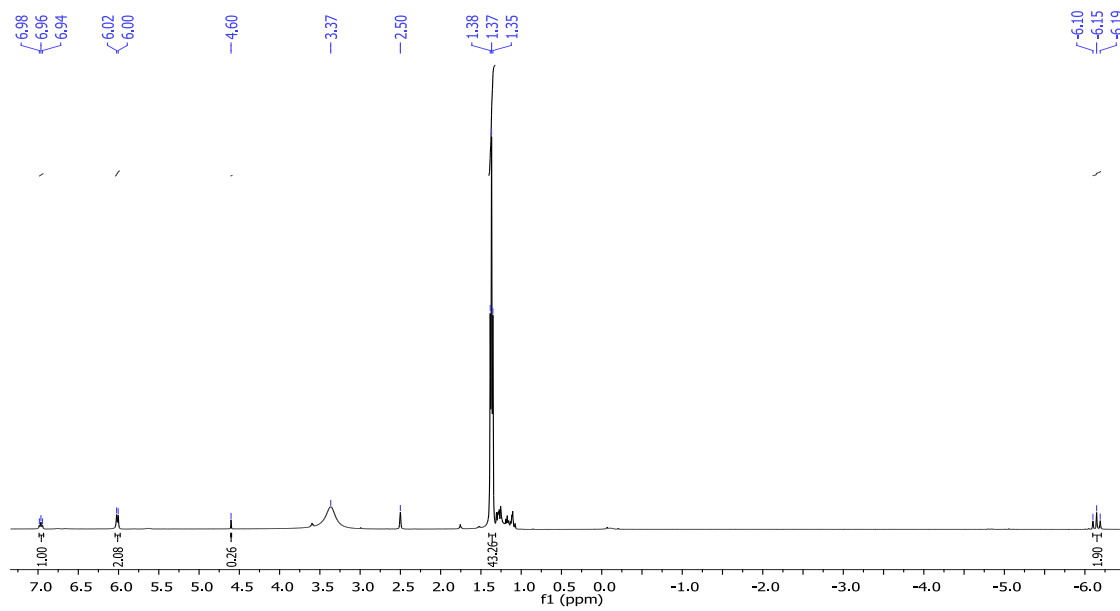


Figure S4. ^{31}P NMR spectrum of **3** in $\text{DMSO-}d_6$ (162.5 MHz, 25 °C).



Scheme S2

Figure S5. 1H NMR spectrum **5** in $DMSO-d_6$ (400 MHz, 25 $^{\circ}C$).

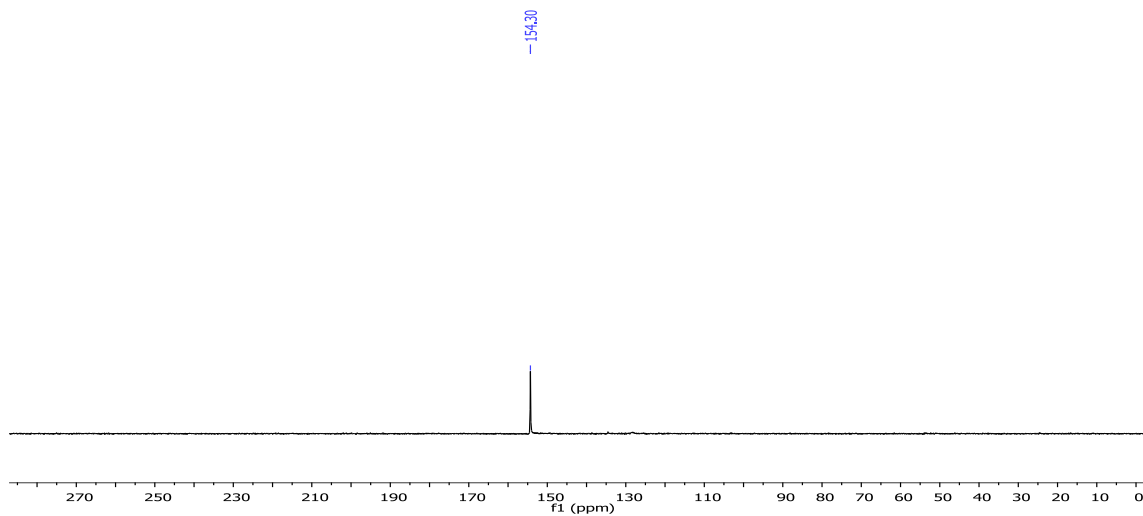


Figure S6. ³¹P NMR spectrum of **5** in DMSO-*d*₆ (162.5 MHz, 25 °C).

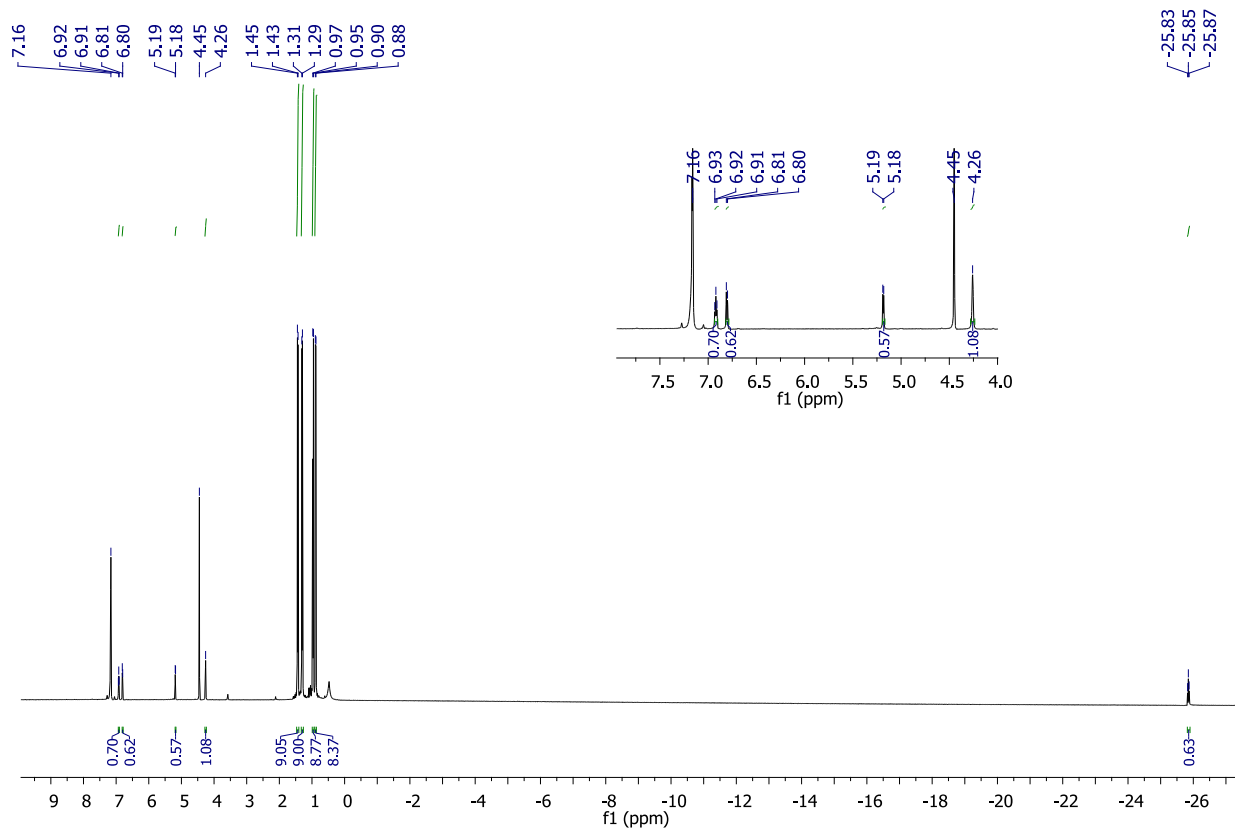


Figure S7. ¹H NMR spectrum of **3** with H₂ in C₆D₆ (400 MHz, 25 °C).

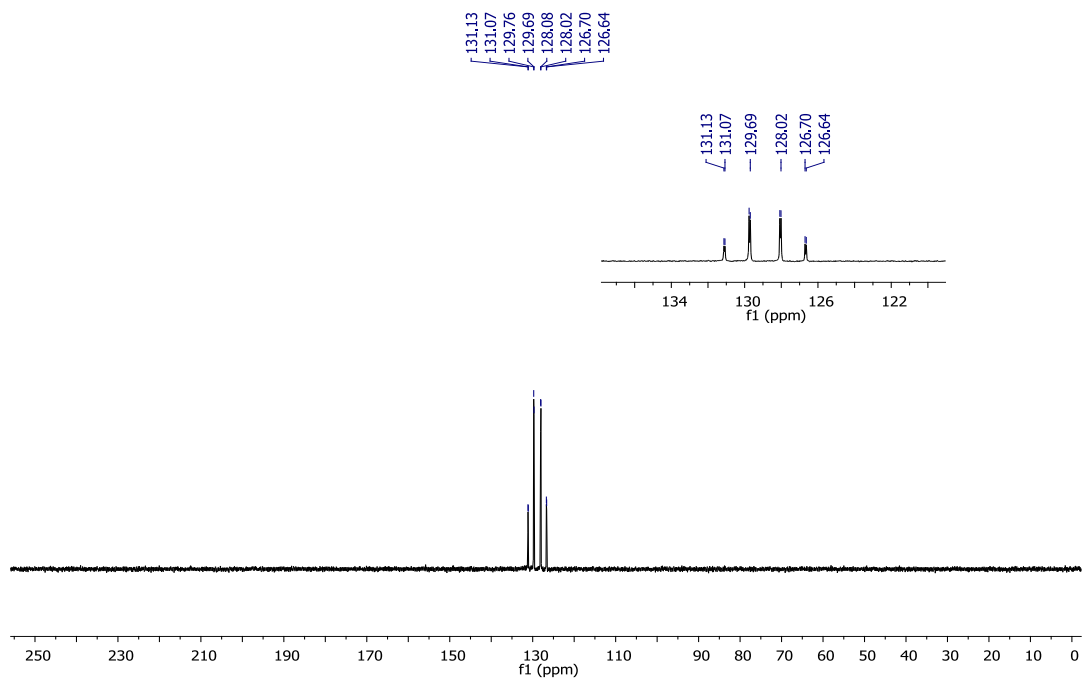
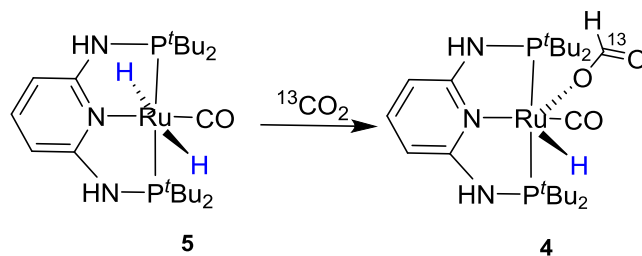
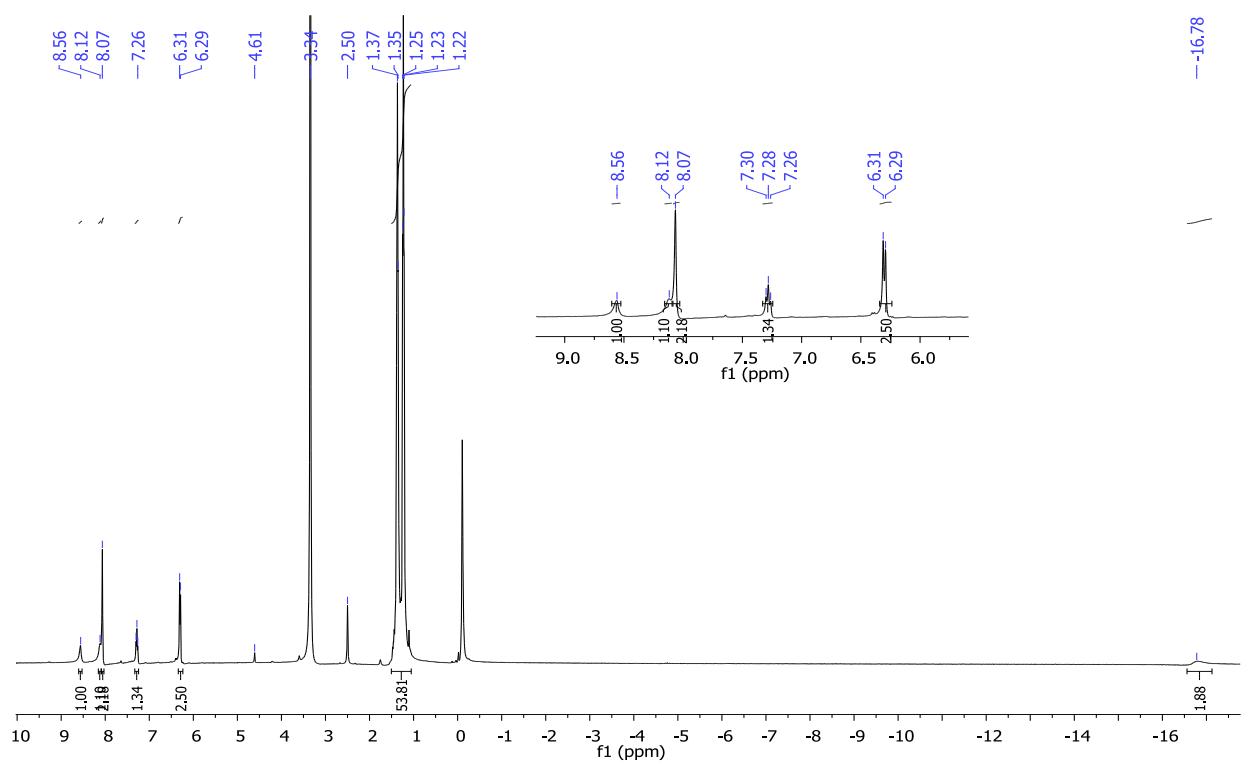


Figure S8. ^{31}P NMR spectrum of **3** with H_2 in C_6D_6 (162.5 MHz, 25 °C).



Scheme S3

Figure S9. ^1H NMR spectrum of **4** in $\text{DMSO-}d_6$ (400 MHz, 25 $^\circ\text{C}$).

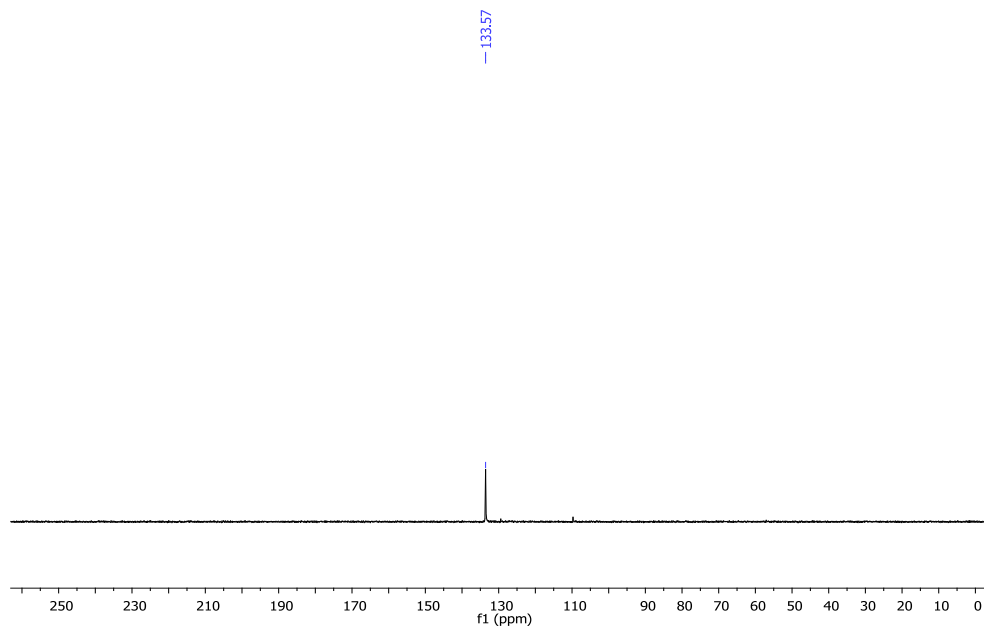


Figure S10. ^{31}P NMR spectrum of **4** in $\text{DMSO-}d_6$ (162.5 MHz, 25 °C).

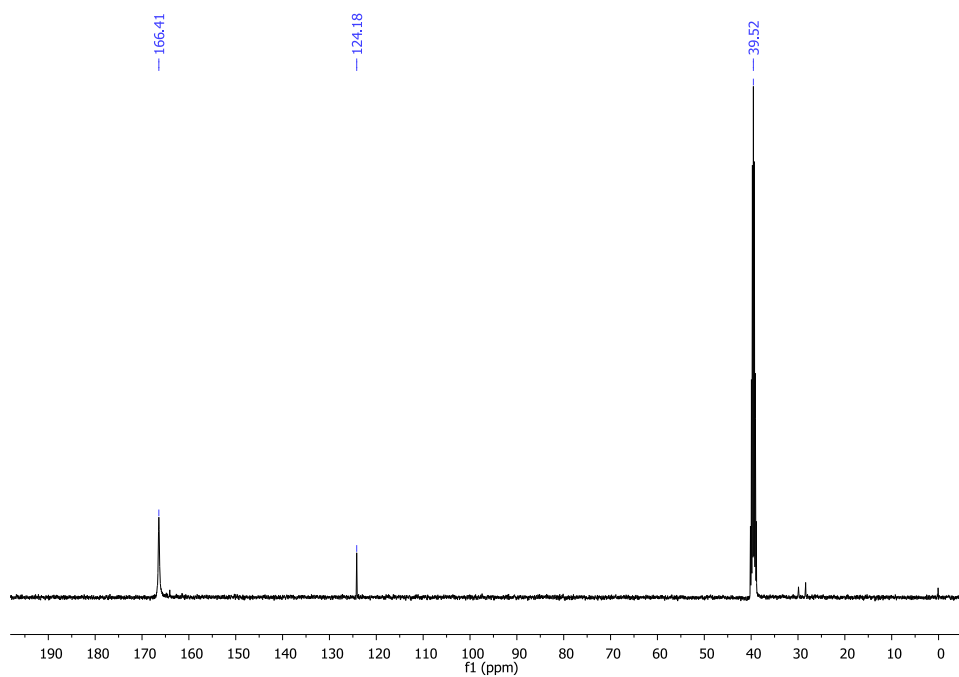
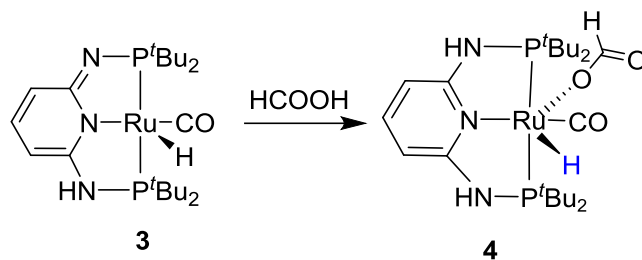
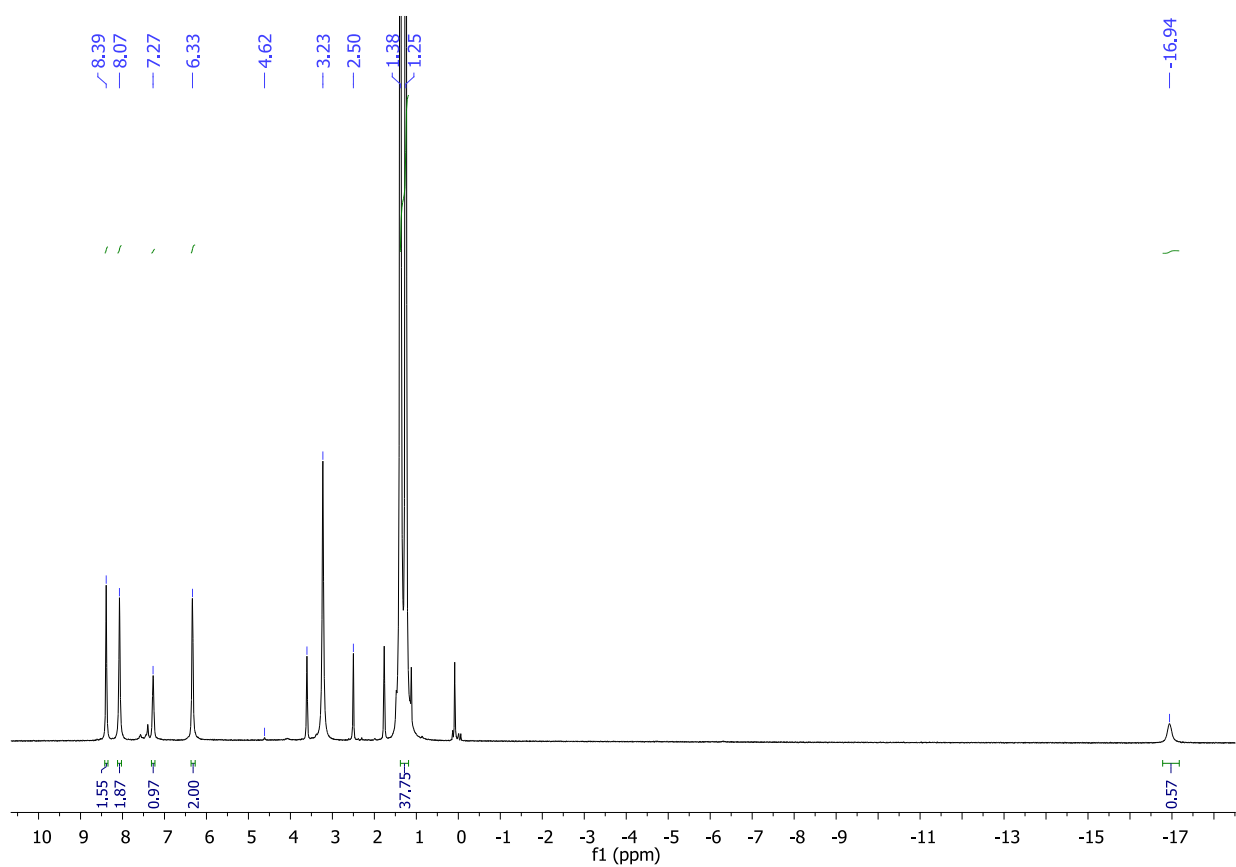


Figure S11. ^{13}C NMR spectrum of **4** in $\text{DMSO-}d_6$ (100 MHz, 25 °C, ns = 512).



Scheme S4

Figure S12. ^1H NMR spectrum **4** in $\text{DMSO-}d_6$ (400 MHz, 25 °C).

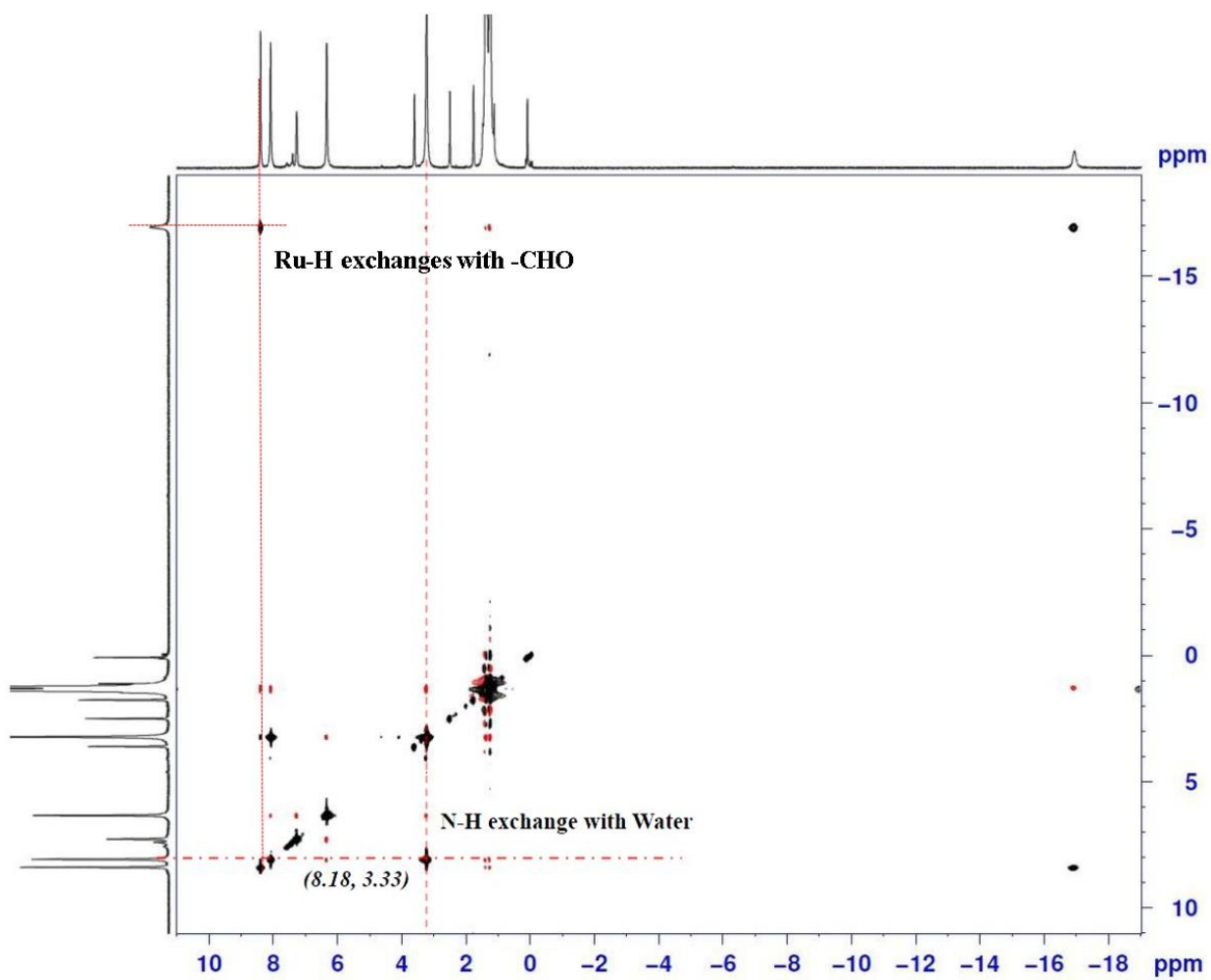
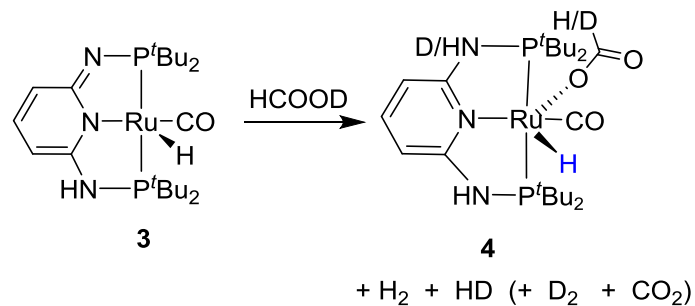


Figure S13. H-H 2D NOESY NMR spectrum of **4** in DMSO- d_6 .



Scheme S5

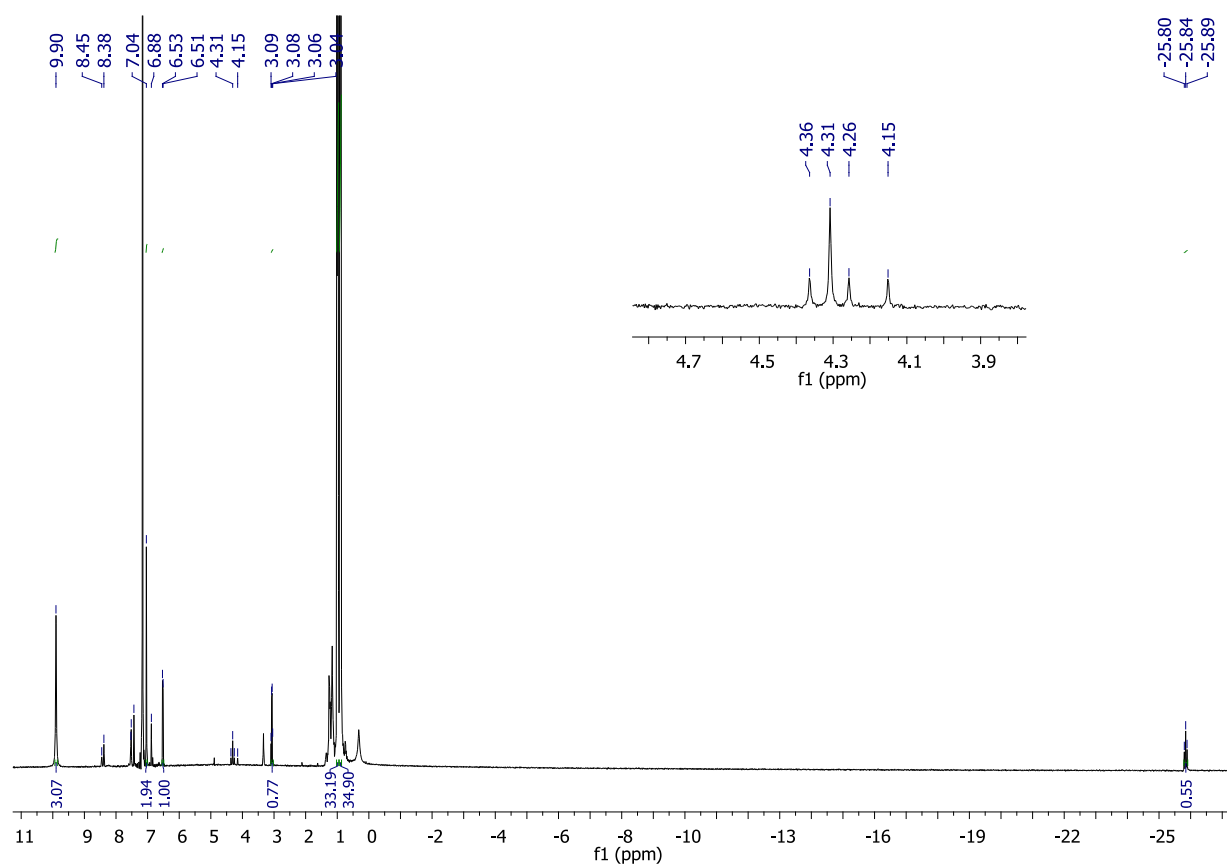


Figure S14. ^1H NMR spectrum of **3** with HCOOD in C_6D_6 (400 MHz, 25 °C).

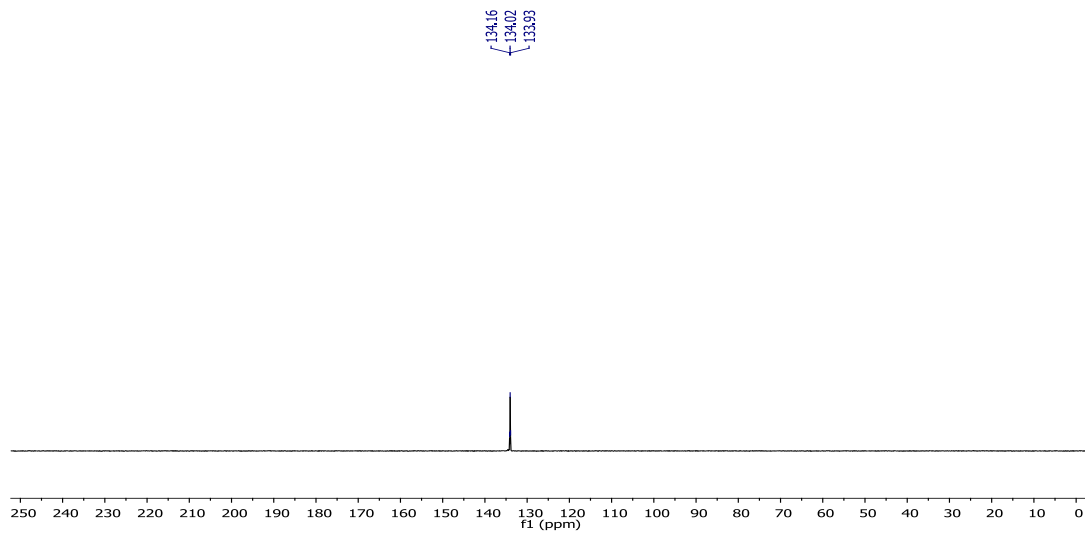


Figure S15. ^{31}P NMR spectrum of **3** with HCOOD in C_6D_6 (162.5 MHz, 25 °C).

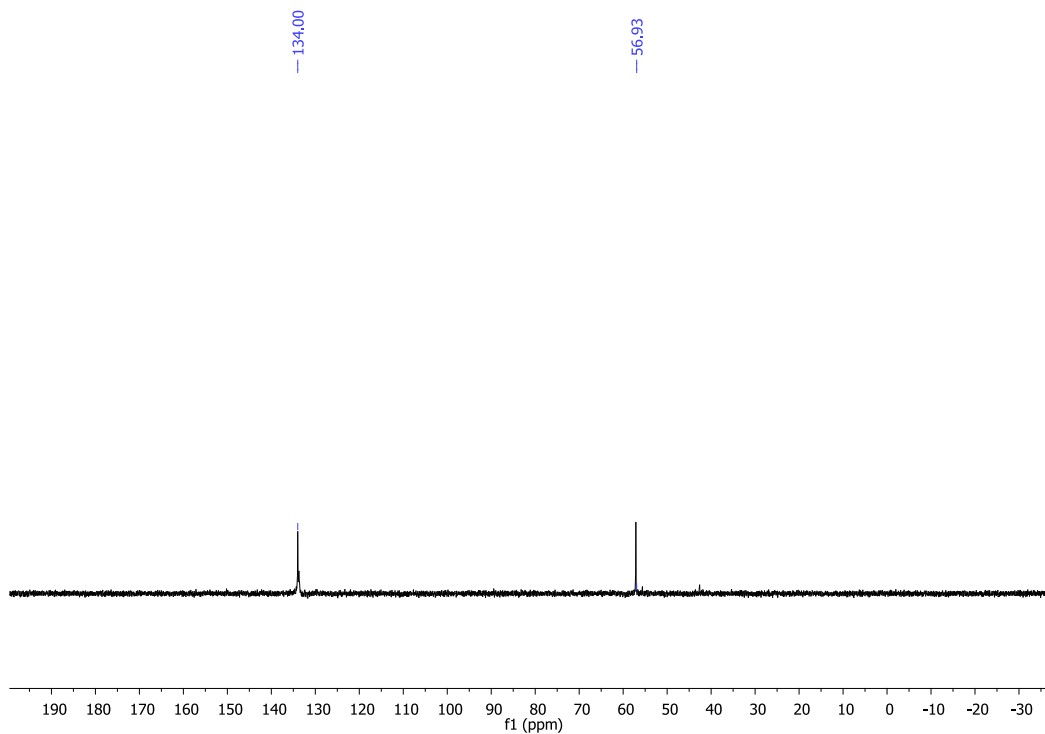


Figure S16. ^{31}P NMR spectrum of **3** which decomposed in the presence of excess HCOOH in $\text{DMSO}-d_6$ (256 MHz, 25 °C).

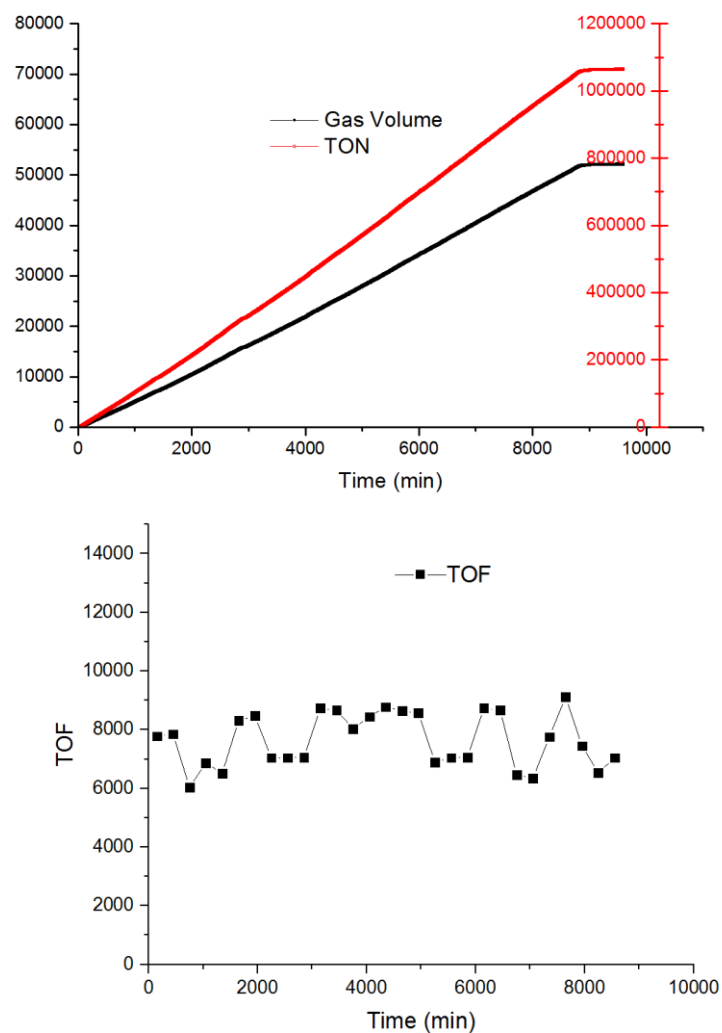


Figure S17. Time-dependent performance of catalyst **3**. Reaction conditions: **3** (1.0 μmol , 1.0 mL DMSO solution), 90 $^{\circ}\text{C}$, DMSO (0.7 mL), NEt_3 (1.5 mL), the flow rate of FA is 0.30 mL/h. Gas volume was recorded in mL.

Author Manuscript

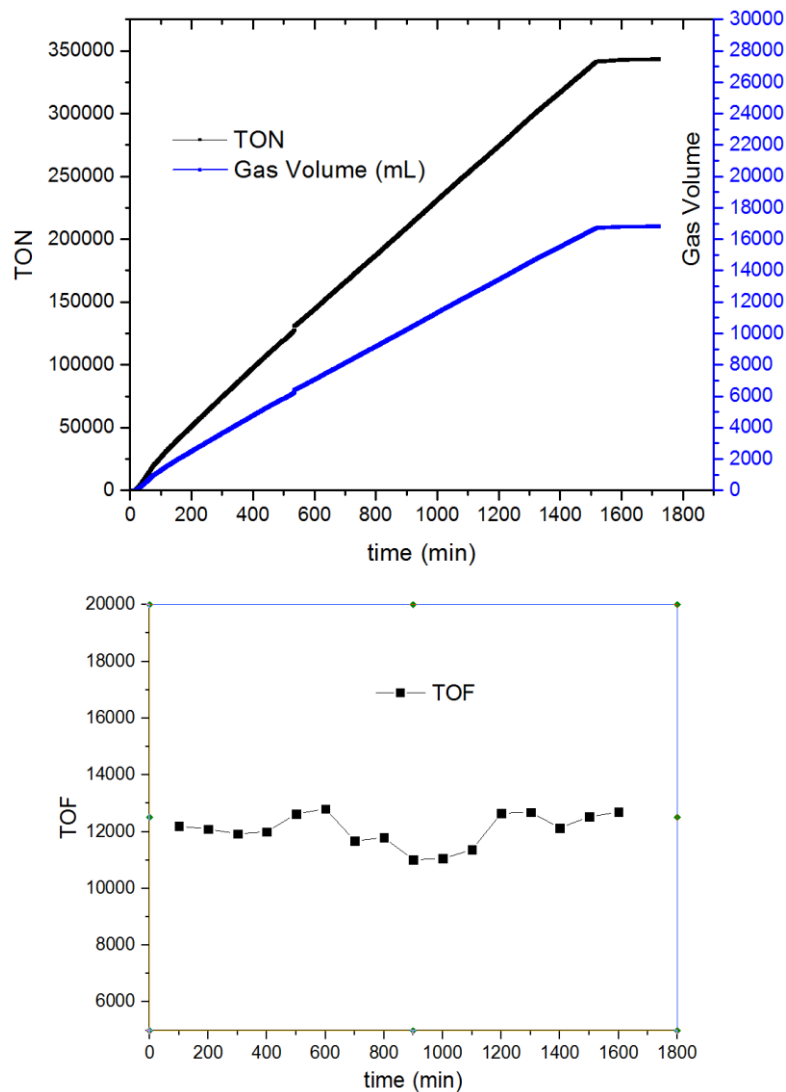


Figure S18. Time-dependent performance of catalyst **3**. Reaction conditions: **3** (1.0 μmol , 1.0 mL DMSO solution), 90 $^{\circ}\text{C}$, DMSO: 5.0 mL, Na_2CO_3 0.624 g, the total volume of FA injection was 14.5 mL, in the first 3 hours, the injection rate was 1 mL/hour, then the rate was changed to 0.5 mL/hour). Gas volume was recorded in mL.